



# TP-AGB stars with envelope burning

P. Marigo<sup>1</sup>, A. Bressan<sup>2</sup>, and C. Chiosi<sup>3,1</sup>

<sup>1</sup> Department of Astronomy, University of Padova, Vicolo dell'Osservatorio 5, 35122 Padova, Italy

<sup>2</sup> Astronomical Observatory, Vicolo dell'Osservatorio 5, 35122 Padova, Italy

<sup>3</sup> European Southern Observatory, K-Schwarzschild-strasse 2, D-85748, Garching bei München, Germany

Received 2 July 1997; accepted 20 October 1997

**Abstract.** In this paper we focus on the TP-AGB evolution of intermediate-mass stars experiencing envelope burning ( $M = 4 \div 5 M_{\odot}$ ). Our model of the TP-AGB phase is suitably designed to follow the peculiar behaviour of these stars, to which the simple analytical treatment valid in the low-mass range can no longer be applied.

The approach we have adopted is a semi-analytical one as it combines analytical relationships derived from complete models of TP-AGB stars with sole envelope models in which the physical structure is calculated from the photosphere down to the core. The solution for the envelope models stands on an original numerical method which allows to treat major aspects of envelope burning.

The method secures that, during the quiescent interpulse periods, fundamental quantities such as the effective temperature, the surface luminosity, the physical structure of the deepest and hottest layers of the envelope, and the related energy generation from nuclear burning, are not input parameters but the consequence of envelope model calculations. This minimizes the use of analytical relations, thus giving our results greater homogeneity and accuracy.

Moreover, we would like to draw the attention on the general validity of our algorithm which can be applied also to the case of low-mass stars, in which envelope burning does not occur.

Our efforts are directed to analyse the effects produced by envelope burning, such as: i) the energy contribution which may drive significant deviations from the standard core mass-luminosity relationship; and ii) the changes in the surface chemical composition due to nuclear burning via the CNO cycle.

Evolutionary models for stars with initial mass of 4.0, 4.5, 5.0  $M_{\odot}$  and two choices of the initial chemical com-

position ( $[Y = 0.28, Z = 0.02]$  and  $[Y = 0.25, Z = 0.008]$ ) are calculated from the first thermal pulse till the complete ejection of the envelope. We find that massive TP-AGB stars can rapidly reach high luminosities ( $-6 > M_{\text{bol}} > -7$ ), without exceeding, however, the classical limit to the AGB luminosity of  $M_{\text{bol}} \simeq -7.1$  corresponding to the Chandrasekhar value of the core mass. No carbon stars brighter than  $M_{\text{bol}} \sim -6.5$  are predicted to form (the alternative of a possible transition from M-star to C-star during the final pulses is also explored), in agreement with observations which indicate that most of the very luminous AGB stars are oxygen-rich.

Finally, new chemical yields from stars in the mass range  $4 \div 5 M_{\odot}$  are presented, so as to extend the sets of stellar yields from low-mass stars already calculated by Marigo et al. (1996). For each CNO element we give both the secondary and the primary components.

**Key words:** stars: evolution – stars: AGB and post-AGB – nuclear reactions, nucleosynthesis, abundances – stars: abundances – stars: carbon – ISM: Planetary Nebulae: general

## 1. Introduction

This study deals with the theoretical evolution of TP-AGB stars undergoing envelope burning – i.e. those in which the base of the convective envelope deepens into high temperature regions so that H-burning via the CNO cycle can occur. This circumstance is usually encountered in AGB stars with massive and extended envelopes ( $M_{\text{env}} \gtrsim 2.5 M_{\odot}$ ), as indicated by several authors (Sugimoto 1971; Uus 1972; Iben 1973; Renzini & Voli 1981;

Scalo et al. 1975; Blöcker & Schönberner 1991; Lattanzio 1992; Boothroyd & Sackmann 1992; Vassiliadis & Wood 1993; Blöcker 1995a; Marigo et al. 1996). The most notable signature of the TP-AGB evolution of these stars is the break-down of the core mass-luminosity relation at high luminosities (Blöcker & Schönberner 1991; Lattanzio 1992; Boothroyd & Sackmann 1992).

Previous analyses of the AGB phase performed with the aid of envelope models have already pointed out that nuclear burning can take place in the deepest and hottest layers of the convective envelope (Scalo et al. 1975; Renzini & Voli 1981; Marigo et al. 1996).

In Marigo et al. (1996) we adopted the assumption that those regions do not provide energy to the star, and the constraint that the core mass-luminosity relation is always satisfied.

The notable improvement of the present approach is to account for the energy generated by the burning regions of the envelope. For this purpose, we develop an algorithm to include nuclear burning in the envelope of a star in thermal equilibrium.

Establishing how deep in the interior the convective envelope penetrates is crucial to determine the efficiency of the nucleosynthesis processes, for the extreme sensitivity of nuclear rates to temperature and density. Furthermore, nuclear burning changes not only the chemical composition of the envelope, but also affects the luminosity, the effective temperature, and the radius of the star. Therefore, the calculation of the envelope models must be carried out with great accuracy.

The theoretical approach developed in this study offers some advantages: it keeps the agility of purely analytical models for quick computing and easy testing of different prescriptions but it has greater accuracy and self-consistency, which draw it closer to full calculations of the TP-AGB phase.

This paper is organized in three main sections. In the first part (Sect. 2) we summarize the physical conditions under which the core-mass luminosity relation is found and we analyze the break-down of this due to envelope burning contributing to the total stellar luminosity over the quiescent inter-pulse period (Sect. 3). The theoretical method developed to this aim is described and discussed (Sect. 3.1).

In the second part (Sect. 4) we apply our method to follow the TP-AGB phase of the 4.0, 4.5, 5.0 $M_{\odot}$  stars with two choices of the initial chemical composition, namely  $[Y = 0.25, Z = 0.008]$  and  $[Y = 0.28, Z = 0.02]$ . The calculations are carried out from the end of the E-AGB up to the complete ejection of the envelope.

In the third part (Sect. 5) we study the nucleosynthesis associated to envelope burning which, together with the third dredge-up, concurs to alter the surface abundances of the elemental species. Finally (Sect. 6), we provide new chemical yields from stars in the above mass range, distin-

guishing for each element of the CNO group the primary and secondary contribution.

## 2. The core mass-luminosity relation

Paczynski (1970) first discovered the existence of a simple, almost linear relationship between the core mass of a double-shell burning star and its quiescent inter-flash luminosity along the TP-AGB.

Over the years, continuous upgrading of the input physics (e.g. new opacities, revised nuclear reaction rates, equations of state, etc.) and detailed calculations of the AGB phase for wide ranges of stellar masses and chemical compositions resulted into a flourishing of different core mass-luminosity ( $M_c - L$ ) relationships (Iben 1977; Iben & Truran 1978; Havazelet & Barkat 1979; Wood & Zarro 1981; Lattanzio 1986; Boothroyd & Sackmann 1988a).

In this work (see also Marigo et al. 1996) we adopt the following relations:

$$L_{M_c} = 238\,000\mu^3 Z_{\text{CNO}}^{0.04} (M_c^2 - 0.0305M_c - 0.1802) \quad (1)$$

for stars with core mass in the range  $0.5M_{\odot} \leq M_c \leq 0.66M_{\odot}$  (Boothroyd & Sackmann 1988a); and

$$L_{M_c} = 122585\mu^2 (M_c - 0.46)M^{0.19} \quad (2)$$

for stars with core mass  $M_c \geq 0.95M_{\odot}$  (originally from Iben & Truran 1978 according to the slightly modified version of Groenewegen & de Jong 1993; see also Iben 1977).

In these formulas stellar masses  $M$  and luminosities  $L$  are in solar units;  $Z_{\text{CNO}}$  is the total abundance (in mass fraction) of C, N, O isotopes in the envelope;  $\mu = 4/(5X + 3 - Z)$  is the mean molecular weight under the assumption of a fully ionized gas, where  $X$  and  $Z$  are the abundances of hydrogen and metals, respectively. For stars with core mass  $0.66M_{\odot} < M_c < 0.95M_{\odot}$  a linear interpolation is performed.

In our model we also account for the steep luminosity increment as a function of the core mass during the first inter-pulse periods, before the onset of the “full amplitude” regime to which the standard  $M_c - L$  relation given by Eqs. (1) or (2) refers. The initial subluminescent evolution is followed by adopting a simple linear relation between the luminosity and the core mass,  $L_{\text{first}} = S \times M_c + Q$ , with the slope  $S$  given as a function of the initial mass  $M_i$  of the star:

$$S = 60761.2 \times \exp(M_i/2.) \quad (3)$$

where masses and luminosities are expressed in solar units. This relation is a least-square fit to the results presented by Vassiliadis & Wood (1993) (see their Fig. 12). For each value of  $M_i$ , the intercept  $Q$  is fixed by the values of the luminosity and core mass at the first thermal pulse.

The existence of the core mass-luminosity relation for AGB stars was given a transparent analytical explanation

by Tuchman et al. (1983) just starting from the equations of stellar structure under specific physical conditions (“radiative zero solution”; see Eggleton 1967; Paczynski 1970). The stellar structure is required to possess a degenerate core of mass  $M_c$  surrounded by a narrow radiative shell (or double shell) source providing the luminosity, beyond which there must exist a thin (with a mass  $\Delta M \ll M_c$ ) and inert (the luminosity is constant) *transition region* in radiative equilibrium. This is bounded at the top by the base of the convective envelope. Integrating the equations of hydrostatic and radiative equilibrium over the *transition region*, after simple substitutions, Tuchman et al. (1983) derived an analytical expression relating the luminosity  $L$  of the star to its core mass  $M_c$ , with some dependence on the chemical composition and the temperature just above the burning shell. The effect of the outer envelope on this relation is negligible because of the extremely steepness of pressure, temperature, and density gradients in the radiative zone. Thus, during the quiescent TP-AGB phase, the evolution of the core is expected to be essentially decoupled from that of the envelope (no mass dependence).

However, Tuchman et al. (1983) suggested that the  $M_c - L$  relation is likely to break down for stars with envelope burning, as the base of the convective envelope may penetrate so deeply as to eat up the radiative buffer over the H-burning shell.

Such a possibility was anticipated by Scalo et al. (1975) who pointed out that, during the quiescent inter-pulse period, in massive and luminous AGB stars the envelope convection may extend all the way down to the H-burning shell, as a result of the high radiation pressure  $P_R$ . In brief, when the contribution of  $P_R$  to the total pressure becomes significant, the radiative ( $\nabla_{\text{rad}}$ ) and adiabatic ( $\nabla_{\text{ad}}$ ) temperature gradients are expected to decrease less steeply with depth, and to reach the minimum value of 0.25, respectively. Both facts concur in drawing the base of the convective envelope – reached when  $\nabla_{\text{rad}} = \nabla_{\text{ad}}$  – deeper in the interior. High temperatures ( $T_b > 40 \times 10^6$  K) can be attained, thus allowing nuclear burning at the base of the envelope.

### 3. Envelope burning as an energy source

Over the years it has become clear that the energy generation due to envelope burning can make massive TP-AGB stars to significantly deviate from the  $M_c - L$  relation. High luminosities are soon reached ( $M_{\text{bol}} < -6$ ), at least until the residual envelope is massive enough to allow for high temperatures ( $T_b > 40 \times 10^6$  K) at its bottom. All this is indicated by complete models of TP-AGB stars (Blöcker & Schönberner 1991; Lattanzio 1992; Boothroyd & Sackmann 1992; Vassiliadis & Wood 1993).

Earlier analyses, primarily aimed to study the structure of envelope burning and associated nucleosynthesis, were carried out with the aid of convective envelopes mod-

els (Scalo et al. 1975; Renzini & Voli 1981). The same kind of theoretical approach adopted in the semi-analytical TP-AGB model by Marigo et al. (1996). The assumption common to all those models is that the envelope satisfies the classical core mass-luminosity relation. This is no longer valid in massive AGB stars, due to the energy generation by envelope burning. Moreover, numerical integrations were made under the constraint that the radial coordinate of the base of the convective envelope coincides with the core radius (Renzini & Voli 1981; Marigo et al. 1996). This approximation can be risky in the case of massive TP-AGB stars as the base of the convective envelope falls in a region, which is very thin in mass but across which the structural gradients are very steep. Therefore, fixing *a priori* the inner extension of the envelope convection may lead to heavily under- or over-estimate the base temperature, to the value of which the nuclear rates are highly sensitive. In contrast, the correct treatment of the envelope burning requires that the energy being generated by nuclear reactions is taken into account and the exact location of the deepest layer through which external convection penetrates is determined (e.g. by the Schwarzschild condition).

#### 3.1. The method of solution

First of all, we relax the original assumption fixing the local luminosity at a constant value (equal to  $L$ ) throughout the envelope (i.e. no energy source). This condition is replaced with the equation of energy balance:

$$\frac{dL_r}{dr} = 4\pi r^2 \epsilon_r \rho_r \quad (4)$$

where  $L_r$  is the local luminosity;  $\rho_r$  the gas density;  $\epsilon_r$  is the amount of energy released by nuclear transmutation of hydrogen into helium per unit of mass and time. All the variables are evaluated at the radius  $r$ .

The integration of Eq. (4) across the envelope must satisfy the basic constraint given by the principle of energy conservation. This means that during the quiescent inter-pulse period the surface luminosity  $L$  is the sum of different contributions, namely those from: the radiative H-burning shell,  $L_H$ ; the nuclear burning at the base of the convective envelope,  $L_{\text{EB}}$ ; the small contributions from the He-burning shell,  $L_{\text{He}}$ , the gravitational contraction of the core,  $L_G$ , and the rate of energy loss via neutrinos,  $L_\nu$ :

$$L = \int_0^{R_S} \frac{dL_r}{dr} dr = L_G + L_{\text{He}} + L_H + L_{\text{EB}} - L_\nu \quad (5)$$

where  $R_S = \sqrt{L/(4\pi\sigma T_{\text{eff}}^4)}$  is the stellar surface radius. In this study we do not consider neutrino losses. This negative contribution is very small compared to the total luminosity, and it is indeed negligible in low-mass stars (Iben & Tutokov 1984; Köster & Schönberner 1986). In massive cores (i.e.  $M_c \gtrsim 0.8M_\odot$ ), its absolute value may be initially comparable to the gravitational energy release from

core contraction during the quiescent inter-pulse period (Blöcker 1995a,b). However, as the star evolves the core interiors become cooler and more degenerate so that the neutrino luminosity falls again well below the gravothermal luminosity.

Each term (but for  $L_\nu$ ) of the sum in Eq. (5) can be explicitly expressed as:

$$\begin{aligned} L_G + L_{\text{He}} &= \int_0^{R_{\text{core}}} \frac{dL_r}{dr} dr \\ L_H &= \int_{R_{\text{core}}}^{R_{\text{conv}}} \frac{dL_r}{dr} dr \\ L_{\text{EB}} &= \int_{R_{\text{conv}}}^{R_S} \frac{dL_r}{dr} dr \end{aligned} \quad (6)$$

where  $R_{\text{core}}$  is the core radius, here defined as the radius at the bottom boundary of the H-burning shell, and  $R_{\text{conv}}$  is the radial coordinate of the base of the convective envelope. In the system of equations (6) the only quantity that can be directly evaluated with our envelope model is  $L_{\text{EB}}$ , whereas for the other terms we need some analytical prescriptions. We make use, in particular, of the relation

$$L_G + L_{\text{He}} = 2000(M/7)^{0.4} \exp[3.45(M_c - 0.96)] \quad (7)$$

derived from the results of complete calculations of the AGB phase (Iben 1977; see also Groenewegen & de Jong 1993).

As a first approximation, we consider the energy contribution from envelope burning,  $L_{\text{EB}}$ , as a correction term which is added to the luminosity  $L_{M_c}$  predicted by the  $M_c - L$  relation, Eqs. (1) and (2), to get the total luminosity, i.e.  $L \sim L_{M_c} + L_{\text{EB}}$ . Substituting  $L$  into Eq. (5), we can express the luminosity provided by the radiative H-burning shell as:

$$L_H = L_{M_c} - L_G - L_{\text{He}} \quad (8)$$

There is one aspect of the above scheme deserving some remarks. We have assumed that  $L_H$  and  $L_{\text{EB}}$  are decoupled, whereas in a real star with envelope burning as soon as the envelope convection penetrates into the H-burning region the two luminosities are related to each other in a way that cannot be ascertained *a priori* without calculating a complete stellar model. A possible way out of this difficulty could be a scheme in which the structure of the radiative double-shell source with “deep envelope” is integrated down to the carbon-oxygen core. This approach could be explored in a future study. On the other hand, a preliminary analysis shows that the relative error of our approximation for  $L_H$  (see Eq. (8)) with respect to the results from full AGB calculations is mostly comprised within  $\sim 2\% \div 10\%$  (Marigo 1998, in preparation).

However, despite the adopted approximation, the present model is a step forward when compared with previous analyses of envelope burning performed with the

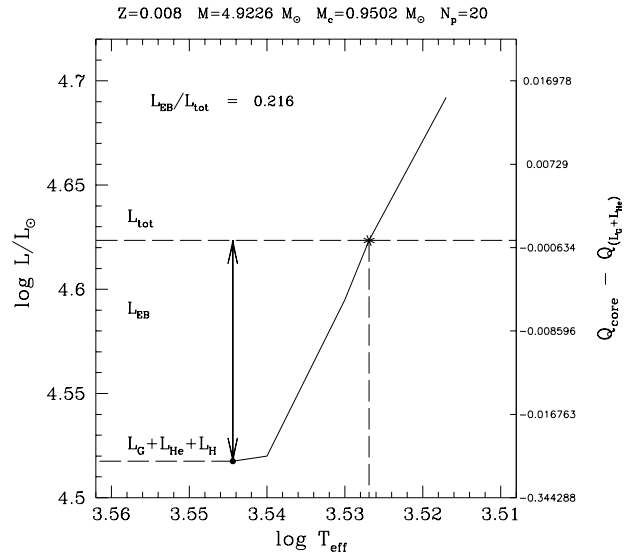


**Fig. 1.** Solution of the system of two equations (12) in the plane  $L - T_{\text{eff}}$ . The solid line corresponds to the locus where  $F(L, T_{\text{eff}}) = 0$  ( $L(R_{\text{conv}}) = L_{M_c}$ ); the asterisk marks the point (solution) where  $G(L, T_{\text{eff}}) = 0$  ( $Q_{\text{core}} = Q_{(L_{\text{He}} + L_G)}$ ).

aid of purely analytical assumptions (Groenewegen & de Jong 1993), or static envelope models (Marigo et al. 1996). Moreover, the results obtained with this scheme turn out to be consistent with those from full evolutionary calculations.

### 3.2. Boundary conditions

Given the stellar mass  $M$ , the core mass  $M_c$ , the chemical composition of the envelope, the luminosities  $L_H$ ,  $L_{\text{He}}$ ,  $L_G$  at a certain time, the task is to find  $T_{\text{eff}}$  and  $L_{\text{EB}}$  (and hence total luminosity  $L$ ) of the stellar model satisfying Eq. (5). The solution is univocally singled out by means of envelope integrations constrained by two boundary conditions, which naturally derive from the system of equations (6) :

$$L(R_{\text{core}}) = L_G + L_{\text{He}} \quad (9)$$

$$L(R_{\text{conv}}) = L_G + L_{\text{He}} + L_H \quad (10)$$

We define the variable  $Q(r) = M(r)/M$  as the mass coordinate of the layer of radius  $r$ , where  $M(r)$  is the mass contained below it and  $M$  is the total stellar mass. Let us call  $Q_{\text{core}}$  and  $Q_{(L_{\text{He}} + L_G)}$  the mass coordinates of the core and of the layer with a luminosity  $L_{\text{He}} + L_G$ , respectively. According to the adopted definition of the core, it is physically equivalent to replace Eq. (9) with:

$$Q_{\text{core}} = Q_{(L_{\text{He}} + L_G)} \quad (11)$$

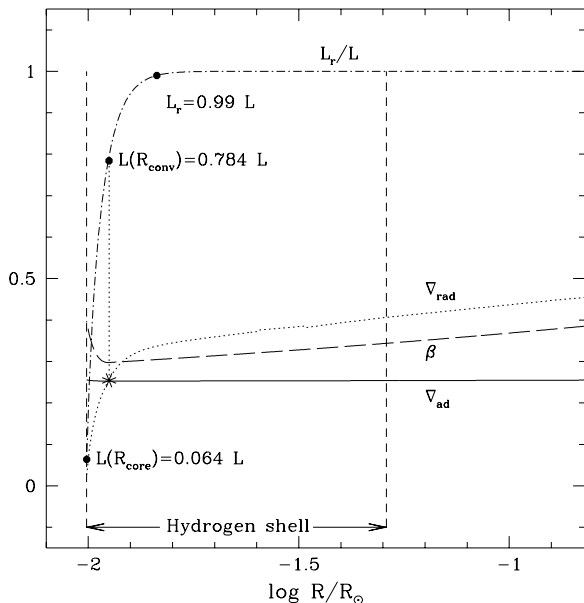


**Fig. 2.** Physical conditions in the deepest layers of the model corresponding to the case illustrated in Fig. 1. The variables  $\nabla_{\text{rad}}$ ,  $\nabla_{\text{ad}}$ ,  $\beta = P_{\text{gas}}/P$ ,  $L_r/L$  are plotted as function of the radial coordinate. The arrows indicate the width of the H-burning shell, with the upper boundary defined by an energy generation rate of  $10 \text{ erg gr}^{-1} \text{ s}^{-1}$ . A few values of the fractional luminosity  $L_r/L$  are displayed at interesting points (marked by full circles), namely: i) the inner boundary of the H-burning shell at  $R_{\text{core}}$ ; ii) the base of the convective envelope (when  $\nabla_{\text{rad}} = \nabla_{\text{ad}}$ , asterisk) at  $R_{\text{conv}}$ ; and iii) the level at which the local luminosity amounts to the 99% of the total luminosity. In this case the envelope convection extends deeply in the interior of the H-burning shell.

which is more suited to our calculations. To summarize, we deal with two boundary conditions (Eqs. (10) and (11)), which require to solve a system of two equations in the two unknowns  $L$  and  $T_{\text{eff}}$ :

$$\begin{cases} G(L, T_{\text{eff}}) = Q_{\text{core}} - Q_{(L_{\text{He}}+L_{\text{G}})} = 0 \\ F(L, T_{\text{eff}}) = L(R_{\text{conv}}) - (L_{\text{G}} + L_{\text{He}} + L_{\text{H}}) = 0 \end{cases} \quad (12)$$

The adopted numerical technique is Brent's method for root finding (Numerical Recipes 1990) applied to both functions. A tolerance  $\epsilon_L = 10^{-5}$  on the root of function  $F$  (expressed as the difference of logarithmic luminosities), seems reasonable for our purposes. Because of the extreme steepness of the structural variables across the H-burning shell, we need to work with a high accuracy,  $\epsilon_Q = 10^{-6}$ , on the root of function  $G$ , such that iterations will continue until  $|Q_{\text{core}} - Q_{(L_{\text{He}}+L_{\text{G}})}| < \epsilon_Q$ .

This method proves to be general and able to work also when envelope burning is not operative, e.g. in the final stages of high mass stars when the mass of the residual envelope is drastically reduced, or in the whole TP-AGB evolution of low-mass stars which never deviate from the

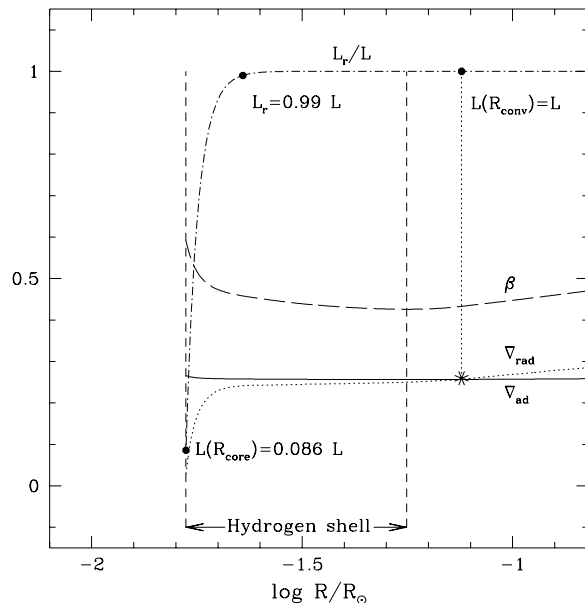


**Fig. 3.** The same as in Fig. 2, but referred to the stage soon after the end of the E-AGB phase. In this case a radiative transition region exists between the upper boundary of the H-burning shell and the base of the convective envelope so that the core mass-luminosity relation still holds.

$M_c - L$  relation. In these cases  $L_{\text{EB}} = 0$  so that the local luminosity all over the envelope coincides with the surface luminosity given by  $L = L_{M_c}$ . The only unknown quantity is then  $T_{\text{eff}}$  which is the root of the function  $G(L_{M_c}, T_{\text{eff}})$ .

In order to show how the method works, we consider the case of a stellar model with current mass  $M = 4.9226 M_{\odot}$ , core mass  $M_c = 0.9502 M_{\odot}$ , and luminosity  $\log L_{M_c} = 4.5175$ , this latter being derived from the  $M_c - L$  relation. These values refer the final stage of the 20<sup>th</sup> inter-pulse period of a  $5 M_{\odot}$ ,  $[Y = 0.25, Z = 0.008]$  star. In the  $\log L - \log T_{\text{eff}}$  plane of Fig. 1 we show the locus (solid line) of the models satisfying the condition  $F = 0$  of Eq. (10). Each  $i^{\text{th}}$  point along the line is derived from envelope integrations carried out with an input luminosity  $L_i = (L_{\text{G}} + L_{\text{He}} + L_{\text{H}}) + \Delta L_i$ , where  $\Delta L_i$  is an arbitrary amount of extra-luminosity. At given  $L_i$  there is a unique value of the effective temperature,  $T_{\text{eff},i}$  (hence a unique envelope model) root of the function  $F$ . Along the right-hand side vertical axis, several values of the function  $G$  - e.g.  $G(L_i, T_{\text{eff},i})$  - derived from envelope models satisfying the condition  $F = 0$  are displayed in a one-to-one correspondence with the luminosity.

The solution of the system of Eqs. (12) is represented by the pair of values  $(\log L = 4.62342, \log T_{\text{eff}} = 3.52689)$  at which both  $F = 0$  and  $G = 0$ . This is indicated by the asterisk along the solid line. In this particular model, the contribution from envelope burning,  $L_{\text{EB}}$ , amounts to  $\sim 22\%$  of the total luminosity.

Figure 2 shows a few physical quantities characterizing the structure of this model in the deepest regions of the envelope and beyond, down to the lower boundary of the H-burning shell,  $R_{\text{core}}$ . To be noticed is that the base of the convective envelope is reached in the deep interior of the H-burning shell, where the temperature is  $T_b \sim 100 \times 10^6$ .

For comparison, the same quantities are plotted in Fig. 3, but relative to the  $5M_{\odot}$ ,  $[Y = 0.25, Z = 0.008]$  star soon after the end of the E-AGB phase, with  $M_c = 0.9344M_{\odot}$ ,  $\log T_{\text{eff}} = 3.5583$ , and  $L_{M_c} = 4.3502L_{\odot}$ . At this stage, envelope burning is very weak ( $T_b \sim 24 \times 10^6$ ;  $L_{\text{EB}} = 0$ ), so that the star still obeys the  $M_c - L$  relation. Note the existence of the radiative buffer between the H-burning shell and the base of the convective envelope.

#### 4. Evolutionary calculations

With the method described in Sect. 3.1 we calculated the TP-AGB evolution of stars with initial mass of 4.0, 4.5, 5.0  $M_{\odot}$  and two choices of the chemical composition  $[Y = 0.28, Z = 0.02]$  and  $[Y = 0.25, Z = 0.008]$ . In the following we briefly recall the basic ingredients adopted in the model, the same ones employed by Marigo et al. (1996) to whom the reader should refer for more details.

The initial conditions at the first thermal pulse are taken from full evolutionary calculations extending from the main sequence till the beginning of the TP-AGB phase kindly provided us by Léo Girardi (1997, private communication). For each stellar mass we single out the first significant pulse, usually defined as the first He-shell flash in which  $L_{\text{He}}^{\text{max}} > L$ , where  $L$  is the surface luminosity (Boothroyd & Sackmann 1988b). All the quantities of interest are then referred to the time corresponding to the quiescent pre-flash luminosity maximum in the light curve. This procedure let us account for the changes in the surface chemical composition caused by the previous mixing processes, namely, the first dredge-up as the star first reaches its Hayashi track after central hydrogen exhaustion, and the second dredge-up at the base of the E-AGB (Tables 2 and 3).

It is worth noticing that the input physics of our envelope model is the same as in the Padua stellar evolution code, so that our results on the TP-AGB phase are homogeneous with the previous evolutionary history. The main characteristics of these stellar models can be summarized as follows:

- The stellar models in usage here to derive the initial conditions allow for convective overshoot from the core and external envelope (Alongi et al. 1993; see also Marigo et al. 1996). Therefore, the maximum initial mass,  $M_{\text{up}}$ , for a star to build an electron-degenerate C-O core, i.e. to evolve through the AGB phase, is around  $5M_{\odot}$ . Classical models without overshoot predict a higher value, i.e.  $M_{\text{up}} \sim 8M_{\odot}$ .

- The high-temperature opacities are those of Iglesias & Rogers (1996). They are particularly suitable to AGB calculations inclusive of the third dredge-up as the authors also provide tables for a variety of carbon- and oxygen-rich mixtures. At low temperatures ( $T < 10^4 K$ ) we use the molecular opacities of Alexander & Ferguson (1994).
- In the outermost super-adiabatic convective region, the adopted value of the mixing length parameter is  $\alpha = 1.68$ , according to the calibration of the solar model.
- Finally, the CNO-cycle nuclear reaction rates are from Caughlan & Fowler (1988).

The analytical relations used to construct our TP-AGB synthetic model are:

- (1) *The core mass-luminosity relation*, given by Eq. (1) or Eq. (2).
- (2) *The core mass-interpulse period relation*, taken from Boothroyd & Sackmann (1988b):

$$\log T_{\text{ip}} = \begin{cases} 4.50 (1.689 - M_c) & \text{for } Z = 0.02 \\ 4.95 (1.644 - M_c) & \text{for } Z = 0.001 \end{cases} \quad (13)$$

where  $T_{\text{ip}}$  and  $M_c$  are expressed in years and solar units, respectively.

- (3) *The rate of evolution*, according to Groenewegen & de Jong (1993):

$$\frac{dM_c}{dt} = 9.555 \cdot 10^{-12} \frac{L_{\text{H}}}{X} \quad (14)$$

where  $dM_c/dt$  is the growth rate of the core mass ( $M_{\odot} \text{yr}^{-1}$ ),  $X$  is the hydrogen abundance (in mass fraction) in the envelope,  $L_{\text{H}}$  is the luminosity produced by H-burning (in solar units). The numerical factor takes into account the energy released from the nuclear conversion of 1 g of hydrogen into helium ( $\sim 6.4 \cdot 10^{18} \text{ erg}$ ).

(4) *Flash-driven luminosity variations* – We apply proper corrections as a function of the envelope mass (Groenewegen & de Jong 1993) to account for the deviations in the luminosity caused by the occurrence of thermal pulses, i.e. the post-flash luminosity peak and the low-luminosity dip.

(5) *Mass loss* – The adopted prescription for the mass-loss rate is the semi-empirical one of Vassiliadis & Wood (1993), which gives the rate as a function of the pulsational period of variable AGB stars:

$$\log \dot{M} = -11.4 + 0.0123P \quad (15)$$

$$\dot{M} = 6.07023 \cdot 10^{-3} \frac{L}{cv_{\text{exp}}}, \quad (16)$$

Here,  $\dot{M}$  is given in units of  $M_{\odot} \text{yr}^{-1}$ , the stellar luminosity  $L$  is expressed in  $L_{\odot}$ , the pulsation period  $P$  in days,  $c$  is the light speed (in  $\text{km s}^{-1}$ ) and  $v_{\text{exp}}$  (in  $\text{km s}^{-1}$ ) denotes the terminal velocity of stellar wind. During calculations,

at any time step, the mass-loss rate is chosen to be the minimum value between those given by Eq. (15) and (16). The wind expansion velocity  $v_{\text{exp}}$  (in  $\text{km s}^{-1}$ ) is estimated as a function of the period of pulsation:

$$v_{\text{exp}} = -13.5 + 0.056P \quad (17)$$

with the additional constraint that  $v_{\text{exp}}$  lies in the range  $3.0 - 15.0 \text{ km s}^{-1}$ , the upper limit being the typical terminal velocity detected in high mass-loss rate OH/IR stars.

The pulsation period  $P$  is derived from the period-mass-radius relation (Eq. (4) in Vassiliadis & Wood 1993), with the assumption that variable AGB stars are pulsating in the fundamental mode:

$$\log P = -2.07 + 1.94 \log R - 0.9 \log M \quad (18)$$

where the period  $P$  is given in days; the stellar radius  $R$  and mass  $M$  are expressed in solar units.

For each stellar mass the calculations are carried out starting from the first significant pulse until the envelope mass,  $M_{\text{env}}$  reduces to about  $0.001M_{\odot}$  that hydrodynamical studies suggest to be the critical value at which the pulsational instability (and hence strong mass-loss) ceases (Tuchman et al. 1979). It is worth recalling that full evolutionary calculations show that a model star moves off the AGB when the residual envelope mass is diminished below  $0.01M_{\odot}$  (Schönberner 1983). From the present results it turns out that the reddest point in the H-R diagram (see Fig. 8) is reached when  $M_{\text{env}} \sim 0.8 \div 0.9M_{\odot}$  in all cases studied, with a typical value  $\log T_{\text{eff}} \sim 3.48$  for models with  $Z = 0.008$ , and  $\log T_{\text{eff}} \sim 3.44$  for models with  $Z = 0.02$ . Then, the tracks slowly move toward the blue part of the H-R diagram, lying in the interval  $[3.44, 3.48 + 0.03]$  until  $M_{\text{env}} \sim 0.3 \div 0.4M_{\odot}$ . The final evolution of the models is characterized by a quick decrease of  $T_{\text{eff}}$  (because of the very small envelope mass). However, we do not pretend here to handle the delicate topic about the transition from the AGB to the formation of planetary nebulae, which is beyond the aim of the present study.

The total number of thermal pulses included in each evolutionary calculation is  $N_{\text{P}}^{\text{tot}} = 174$  for the  $[4.0M_{\odot}, Z = 0.008]$  model;  $N_{\text{P}}^{\text{tot}} = 146$  for the  $[4.5M_{\odot}, Z = 0.008]$  model;  $N_{\text{P}}^{\text{tot}} = 129$  for the  $[5.0M_{\odot}, Z = 0.008]$  model. A smaller number of thermal pulses are expected to be suffered by stars with the same initial mass, but lower (e.g. solar) metallicity. Our calculations yield  $N_{\text{P}}^{\text{tot}} = 39$  for the  $[4.0M_{\odot}, Z = 0.02]$  model;  $N_{\text{P}}^{\text{tot}} = 56$  for the  $[4.5M_{\odot}, Z = 0.02]$  model;  $N_{\text{P}}^{\text{tot}} = 83$  for the  $[5.0M_{\odot}, Z = 0.02]$  model.

#### 4.1. Evolution in the $M_c - L$ plane

As already mentioned, the energy contribution from envelope burning makes massive TP-AGB stars to leave the  $M_c - L$  relation during part of their evolution. This effect is illustrated in Figs. 4 and 5. During the initial stages of

the thermally pulsing regime the luminosity evolution is governed by the H-burning shell, just re-ignited after the second dredge-up. As the efficiency of the envelope burning increases, the star can quickly reach higher and higher luminosities (steeply rising parts of the curves), with a rate much greater than expected from the slope of the  $M_c - L$  relation (dashed lines). The luminosity growth goes on as long as the envelope remains massive enough to allow high temperatures at the base of the envelope (see Sect. 4.2 below). When mass loss becomes significant (and envelope burning weakens) the luminosity starts to decline and the star eventually approaches again the  $M_c - L$  relation, where it lies till the end of the AGB phase. This kind of luminosity evolution agrees with the results from full evolutionary calculations of the TP-AGB phase (Boothroyd & Sackmann 1992; Vassiliadis & Wood 1993).

The above trend may of course vary depending on several factors, part of which are intrinsic to the stars, e.g. initial mass and chemical composition, and part to the theoretical model, e.g. mixing formalism, mass-loss prescription, opacities, and nuclear reaction rates (see Renzini & Voli 1981; Sackmann & Boothroyd 1991; Boothroyd & Sackmann 1992, 1993; Blöcker 1995a).

Figures 4 and 5 show the effect on the above trend of mass and chemical composition. The deviation from the luminosity predicted by the  $M_c - L$  relation is more pronounced in more massive stars at fixed metallicity. Let us consider the  $[Y = 0.25, Z = 0.008]$  case (Fig. 4). The maximum relative contribution of envelope burning to the total luminosity  $L_{\text{EB}}/L$  goes from about 0.02 for the  $4.0M_{\odot}$  model, 0.14 for the  $4.5M_{\odot}$  model, up to 0.23 for the  $5M_{\odot}$  model. Concerning this latter, the plot shows how the decline in luminosity depends on the current value of the stellar mass (indicated along the curve), as it is progressively reduced by stellar winds. At higher metallicities (Fig. 5), the overluminosity generated by the envelope burning is much smaller at given initial mass. In the  $[Y = 0.28, Z = 0.02]$  case, the maximum relative contribution is negligible for the  $4.0M_{\odot}$  model (which actually never deviates from the  $M_c - L$  relation), and very small for the  $5.0$  and  $4.5M_{\odot}$  stars, where  $L_{\text{EB}}/L$  amounts to 0.15 and 0.05, respectively.

Concluding this section, we like to briefly comment on the dependence of  $M_c - L$  relation given by Eq. (2) on the current star mass (i.e. the factor  $M^{0.19}$ ). Iben (1977) originally introduced a factor  $M^{0.4}$  to fit the results for the AGB evolution (at constant mass) of his  $7.0M_{\odot}$  star. Subsequently Iben & Truran (1978) reduced the exponent to 0.19 to obtain a compromise with the results of Paczynski (1970).

This dependence is indeed quite weak, and it has in practice no effect for most of the TP-AGB lifetime. However, after the onset of the super-wind, envelope stripping gets so efficient that the weight of the mass factor in Eq. (2) becomes important. In Fig. 4 the final, slow decrease in luminosity at increasing core mass during the last

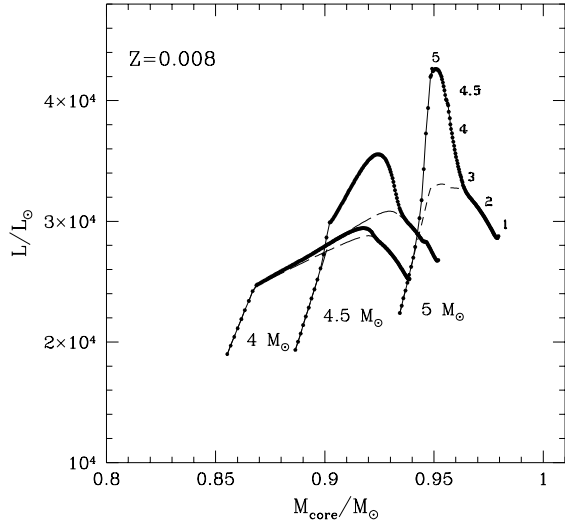


**Fig. 4.** Luminosity evolution of 4.0, 4.5, 5.0  $M_{\odot}$  TP-AGB stars with composition  $[Y = 0.25, Z = 0.008]$  as a function of the core mass. The dashed lines correspond to the standard core mass-luminosity relation, the filled circles refer to the actual stellar luminosity, at its maximum value before each pulse. The overluminosity produced by envelope burning rapidly reaches a maximum value, it starts to decrease after the onset of the super-wind (the numbers along the 5  $M_{\odot}$  curve indicate the current stellar mass in solar units), finally it vanishes and the star approaches again the core mass-luminosity relation.

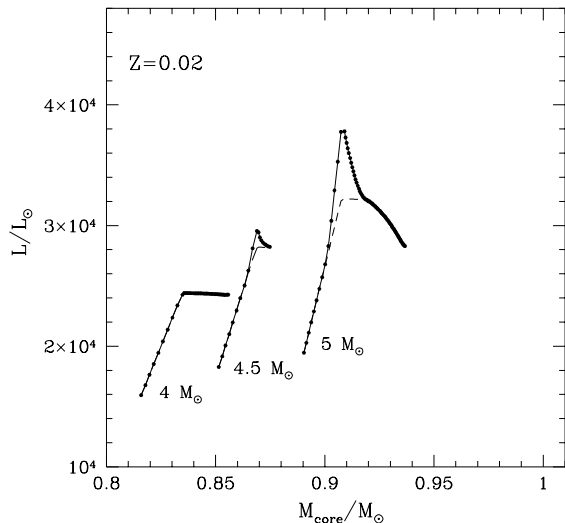


**Fig. 5.** The same as in Fig. 4, but with  $[Y = 0.28, Z = 0.02]$ .

evolutionary stages is just caused by the drastic reduction of the stellar mass.

This trend seems to contradict the existence of the core mass-luminosity relation itself, because this latter implies that the luminosity should not depend on the envelope mass. We may argue that the factor  $M^{0.19}$  actually masked some low-efficiency envelope burning (the adopted mixing length parameter was  $\alpha = 0.7$  in Iben’s calculations, roughly corresponding to  $\alpha \sim 1.4$  of other groups). Though a cautionary remark on the use of such a relation is worthy since it may depend on model details, the general applicability of the our solution scheme is not affected, and the adoption of different  $M_c - L$  relations could be explored in a future study.

#### 4.2. The base temperature

The temperature at the base of the convective envelope,  $T_b$ , is the key-quantity driving the strength of envelope burning. Figures 6 and 7 show  $T_b$  as a function of the pre-flash luminosity maximum for stars with  $[Y = 0.28, Z = 0.02]$  and  $[Y = 0.25, Z = 0.008]$ . Both diagrams share a common trend, regardless of the initial mass and chemical composition (metallicity). Starting from the first pulse, as the star evolves to higher luminosities a rapid increase in  $T_b$  occurs in all models. This feature reflects the progressive inward penetration of the base of the convective envelope, which is essentially driven by the effect of radiation pressure on  $\nabla_{\text{rad}}$  and  $\nabla_{\text{ad}}$  (see Sect. 2). It is worth noticing that in these initial stages, when envelope burning is growing but still weak, there is a well-defined almost linear relation between  $\log T_b$  and  $\log L$ , with a slope nearly independent of the stellar mass.

The subsequent bending of the  $T_b$  curves happens at a certain “threshold luminosity” when the envelope convection eats up the radiative buffer and extends into the H-burning shell (Scalo et al. 1975). This critical luminosity marks the point at which the star begins to deviate from the  $M_c - L$  relation (Figs. 5 and 4). At even higher luminosities, the modest increase in  $T_b$  is controlled by the steep gradient in  $L_r$  (and  $\nabla_{\text{rad}}$  in turn) toward the innermost layers of the burning region. Once the luminosity has reached a maximum value and begins to decline,  $T_b$  lowers as well because of the reduction of envelope mass by stellar winds, and finally it drops so dramatically that envelope burning extinguishes.

Comparing the curves in Figs. 6 and 7 for a given initial mass it turns out that, at the same luminosity, a lower metallicity favours higher values of  $T_b$  along the TP-AGB. A similar effect takes place on the characteristic temperature at which tracks of different metallicities begin to flatten out, with a typical value  $\log T_b \sim 7.73$  for the  $[Y = 0.28, Z = 0.02]$  case and  $\log T_b \sim 7.79$  for the  $[Y = 0.25, Z = 0.008]$  case. Moreover, it is worth remarking that the lower the stellar mass, the lower is the value of the “threshold luminosity”. The 4.0  $M_{\odot}$ ,  $[Y = 0.28, Z = 0.02]$



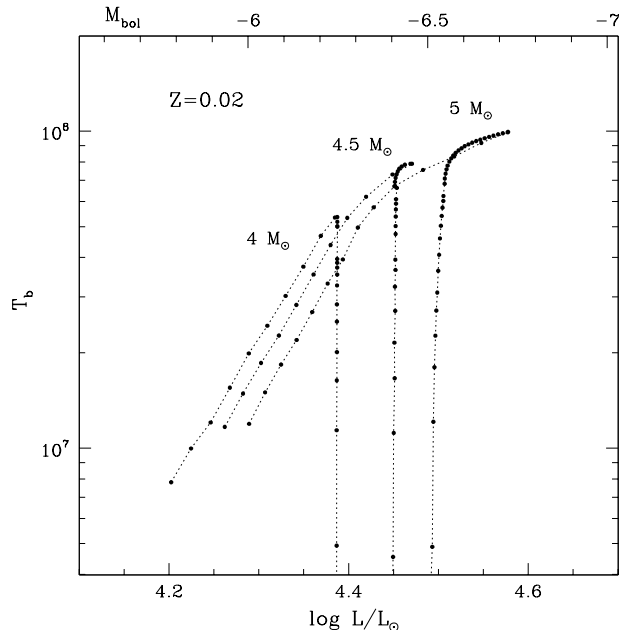


**Fig. 6.** Temperature  $T_b$  at the base of the convective envelope as a function of the pre-flash luminosity maximum (filled circles) for intermediate-mass TP-AGB stars with  $[Y = 0.28, Z = 0.02]$ .

model is a transition case for the occurrence of envelope burning. The flattening of the  $T_b$  curve does not show up because as soon as the star reaches the “threshold luminosity” ( $\log T_b \sim 7.73$ ), the residual envelope is not massive enough to sustain high temperatures at its base. As a consequence of it, the  $T_b$  curve abruptly falls down.

#### 4.3. The H-R diagram

Figure 8 shows the evolutionary tracks in the H-R diagram for our TP-AGB stars with composition  $[Y = 0.25, Z = 0.008]$  (solid lines) and  $[Y = 0.28, Z = 0.02]$  (dotted lines). The first part of the curves shows a well-defined, and almost linear, relation between the luminosity and effective temperature, with a typical slope  $d \log T_{\text{eff}} / d \log L$  around  $-0.13$  for  $[Y = 0.28, Z = 0.02]$  and  $-0.11$  for  $[Y = 0.25, Z = 0.008]$ , and a very small dependence on the initial stellar mass at given metallicity. This feature holds as long as the total stellar mass is not significantly reduced by stellar winds (i.e. up to the luminosity maximum). The subsequent part of the track – corresponding to the decline of the luminosity and quick decrease of the effective temperature – is controlled by the interplay between the weakening of envelope burning and the onset of the superwind phase.

The filled circles show the most luminous AGB stars of a sample of long-period variables in the LMC observed by Wood et al. (1983) in the near infrared pass-bands  $JHK$ . The bolometric magnitudes of the observed stars are re-

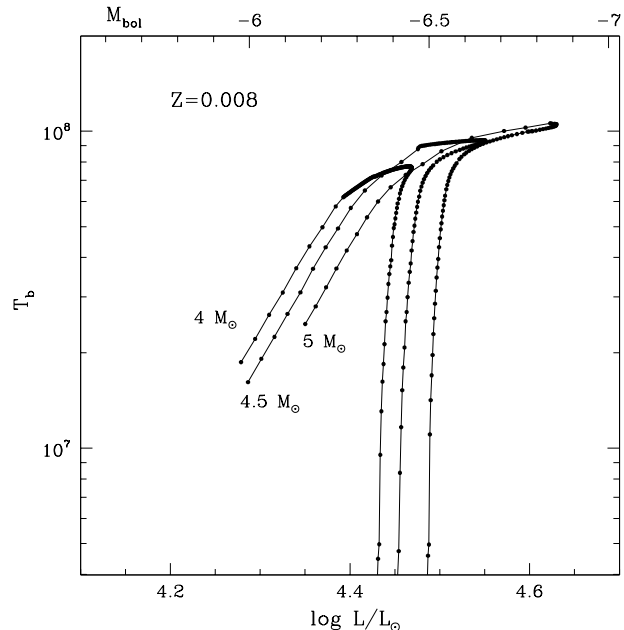


**Fig. 7.** The same as in Fig.6, but with  $[Y = 0.25, Z = 0.008]$ .

scaled to the distance modulus to the LMC,  $(m - M)_o = 18.5$ , instead of 18.6 used by the authors. The conversion of  $(J - K)$  colours to effective temperatures is obtained with the aid of the relation  $T_{\text{eff}} = 7070 / [(J - K) + 0.88]$  from Bessel et al. (1983).

Our tracks for  $[Y = 0.25, Z = 0.008]$  are consistent with the observational data extending in luminosity up to about  $M_{\text{bol}} \sim -7$ . It is worth recalling that all the stars displayed in Fig. 8 are oxygen-rich, in agreement with the expectation from envelope burning, preventing the formation of carbon stars at high luminosities (Sect. 5).

#### 4.4. The $M_{\text{bol}} - P$ diagram

Figure 9 compares in the  $M_{\text{bol}} - P$  diagram theoretical results for TP-AGB stars with different initial mass and composition  $[Y = 0.25, Z = 0.008]$  with the observational data for long-period AGB variables (Mira and OH/IR objects) in the LMC, collected from various authors. Most of the brightest stars are confined below the classical AGB limit, i.e.  $M_{\text{bol}} \sim -7.1$  corresponding to the Chandrasekhar mass  $M_c = 1.4M_\odot$  as predicted by the  $M_c - L$  relation of Paczynski (1970). Furthermore, no theoretical tracks goes beyond this limit. The highest luminosity ( $M_{\text{bol}} \sim -6.85$ ) is reached by the  $5.0M_\odot$ ,  $[Y = 0.25, Z = 0.008]$  model, with a  $M_c \sim 0.95M_\odot$ . The filled triangles indicate some long-period variables which are found by Smith et al. (1995) to possess strong Li features in their spectra. This is usually interpreted as the signature of envelope burning in massive AGB stars (Sect. 5.1). The theoretical results seem to be consistent with the fact that most of the observed stars more lumi-

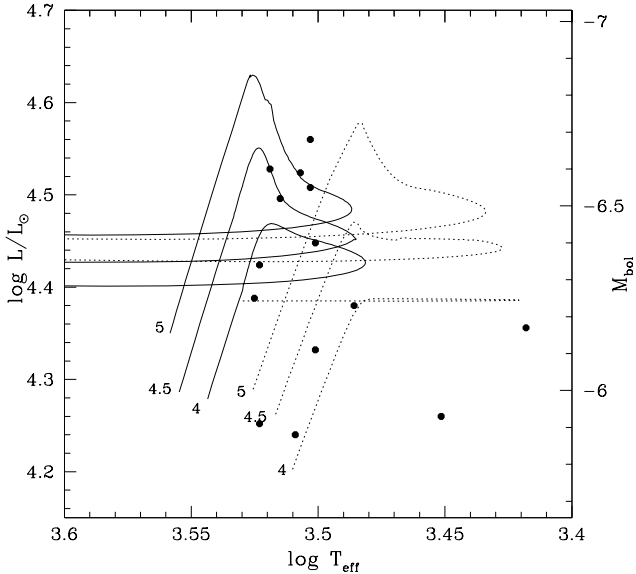


**Fig. 8.** Evolutionary tracks in the H-R diagram for stars with chemical composition  $[Y = 0.25, Z = 0.008]$  (solid lines) and  $[Y = 0.28, Z = 0.02]$  (dotted lines). The numbers indicate the corresponding initial mass in solar units. The filled circles refer to the most luminous oxygen-rich AGB stars in the sample of long-period variables observed by Wood et al. (1983).

nous than  $M_{\text{bol}} \sim -6$  are oxygen-rich. Finally, it is worth noticing that the rapid excursion of the tracks towards very high periods ( $P > 800$  days) occurs when mass loss by stellar winds drastically reduces the envelope mass. In the most massive stars (i.e.  $4.0, 4.5, 5.0M_{\odot}$  models), this stage coincides with the extinction of envelope burning and the recovering of the  $M_c - L$  relation.

## 5. Nucleosynthesis

### 5.1. Observational hints for envelope burning

Envelope burning can heavily alter the surface chemical composition of massive TP-AGB stars via the nuclear reactions of the CNO-cycle (and p-p chain), occurring in convective conditions. Therefore, the chemical abundances observed at the surface of real stars can be used as probes of current theories on the structure and evolution of AGB models.

Over the years a considerable amount of spectroscopic data on the chemical composition of evolved stars has become available, thus setting precise constraints on the nucleosynthesis and mixing processes occurring during the evolution of low- and intermediate-mass stars (Smith & Lambert 1985; Harris et al. 1985, 1987, 1988; Smith & Lambert 1990; Smith et al. 1995).

Depending on the surface abundance ratio C/O, three broad classes of stars can be distinguished: M-giants

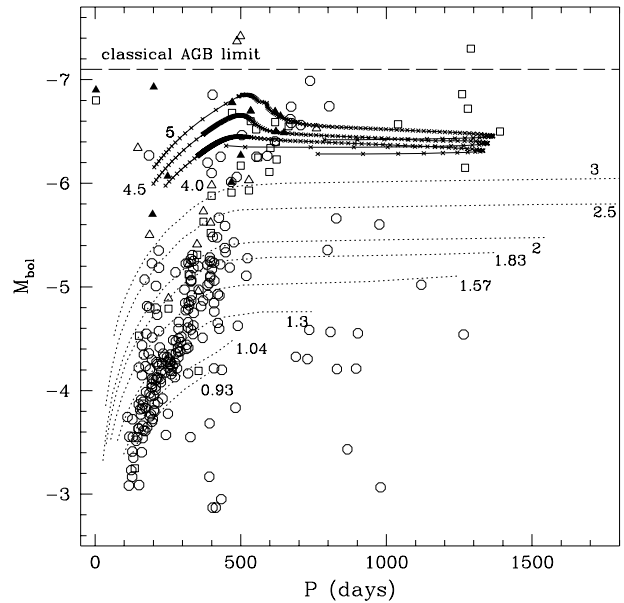


**Fig. 9.** Bolometric magnitude of long-period variable AGB stars as a function of the pulsational period. The data are taken from Smith & Lambert 1990, Smith et al. 1995 (triangles); Wood et al. 1983, Wood et al. 1992 (squares); and Reid et al. 1995 (circles). The theoretical tracks correspond to the evolution of TP-AGB stars with composition  $[Y = 0.25, Z = 0.008]$  for a few representative values of the initial mass (indicated in  $M_{\odot}$  by numbers nearby to the corresponding curve). The dotted lines refer to the results for low-mass stars ( $M \leq 3M_{\odot}$ ), already presented in Marigo et al. (1996).

( $C/O < 0.8$ ), S-giants ( $0.8 \leq C/O < 1.0$ ), and C-giants ( $C/O > 1.0$ ). According to the present understanding, the possible evolutionary sequence along the three classes would be the result of the dredge-up of  $^{12}\text{C}$  at successive thermal pulses. However, the careful analysis of this subject suggests that the real situation is more intriguing and interwoven.

First, a TP-AGB star experiencing envelope burning may not become a carbon star (Boothroyd et al. 1993) because of the rapid conversion of newly dredged-up  $^{12}\text{C}$  into  $^{13}\text{C}$  and then into  $^{14}\text{N}$  via the first reactions of the CNO cycle. This could offer a viable explanation to the observed scarcity of very luminous carbon stars ( $M_{\text{bol}} < -6.5$ ) in the fields of the Galaxy and the fields and clusters of the Magellanic Clouds (Westerlund et al. 1991; Costa & Frogel 1996). Recently, van Loon et al. (1997) have found obscured carbon stars in the Magellanic Clouds at luminosities up to  $M_{\text{bol}} \sim -6.8$ .

Second, stars with envelope burning are expected to rapidly reach high luminosities (Sect. 4.1). This fact would speed up the ejection of the envelope by triggering enhanced mass loss and explain the observed paucity of lumi-

nous oxygen-rich (M-type) stars in the range  $-6 > M_{\text{bol}} > -7$  (Hughes & Wood 1990; Reid et al. 1990).

However, as far as the analogous situation in clusters of the LMC is concerned, there is another effect to be considered, i.e. the effect of the past history of cluster formation in the age range at which AGB stars are expected to occur. In brief, Marigo et al. (1997) have pointed out that the lack of these luminous AGB stars in the youngest LMC clusters could be ascribed to an epoch of modest cluster formation, between ages of  $2 \times 10^8$  and  $6 \times 10^8$  yr ago.

Third, the detailed information on oxygen and carbon isotopic ratios for galactic giant stars have disclosed a more complex scenario (Smith & Lambert 1990) than suggested by the classification based on the C/O ratio. C-stars can be grouped in two sub-classes according to their  $^{12}\text{C}/^{13}\text{C}$  ratio:  $^{13}\text{C}$ -rich J-type ( $^{12}\text{C}/^{13}\text{C} < 10$ ) and N-type ( $^{12}\text{C}/^{13}\text{C} > 10$ ). The low  $^{12}\text{C}/^{13}\text{C}$  ratio in J-type stars, which is very close to the equilibrium value for the CNO cycle, would suggest the occurrence of envelope burning (Renzini & Voli 1981).

In addition to this, extensive spectroscopic searches have been carried out in the Magellanic Clouds to detect lithium in red giant stars (Smith et al. 1995). The Li I 6707 Å resonance line has been measured in AGB stars, mostly belonging to the S-class, within a narrow luminosity range ( $-7 \lesssim M_{\text{bol}} \lesssim -6$ ). This feature is commonly interpreted as the signature of the Cameron & Fowler mechanism for Li production (Cameron & Fowler 1971; Sackmann & Boothroyd 1992) taking place in the typical envelope burning environment. In brief,  $^7\text{Li}$  is produced by electron captures on  $^7\text{Be}$  nuclei convected from the hot regions of the envelope into cooler layers ( $T < 3 \times 10^6 \text{ K}$ ) before the reaction  $^7\text{Be}(p, \gamma)^8\text{B}$  proceeds.

Finally, the expected enrichment in helium and nitrogen caused by envelope burning and mixing episodes is usually invoked to interpret the high He/H and N/O ratios characterizing Planetary Nebulae of Type I (Peimbert & Torres-Peimbert 1983).

### 5.2. The nuclear network: our prescriptions

In this study nuclear burning at the base of the convective envelope is followed adopting the instantaneous mixing approximation. We check that the lifetimes of the CNO nuclei against proton captures are much longer than the time scale for convective turnover in the envelope. This means that the entire envelope is efficiently mixed through the high temperature region at its bottom, so that the new nuclei are redistributed all over the envelope faster than the time scale over which a significant inhomogeneity can be built up (Clayton 1983). At each time, the homogeneous distribution of the nuclei reflects the degree of the CNO cycling attained within the burning zones. To give an example, a surface  $^{12}\text{C}/^{13}\text{C}$  ratio equal or very close to 3.4 implies that the entire envelope has been processed in the deepest regions at sufficiently high temperatures so

that the CN cycle (and possibly the complete CNO cycle) has reached the state of stationary equilibrium.

In the case of long-lived nuclei, the reaction rates can be properly mass-averaged over the whole convective region (Scalo et al. 1975). In contrast in the case of light elements such as  $^7\text{Be}$  and  $^7\text{Li}$  the nuclear lifetimes can be comparable to the convective time scale of the envelope. In such a case the mass-averaging procedure is not meaningful and a time-dependent diffusive algorithm should be employed in order to properly couple nucleosynthesis and mixing.

In the present study the nuclear reactions rates are taken from Caughlan & Fowler (1988). The parameter  $f$  ( $0 \div 1$ ) in their analytical expressions for several uncertain rates such as  $^{15}\text{N}(p, \alpha)^{12}\text{C}$ ,  $^{17}\text{O}(p, \alpha)^{14}\text{N}$ ,  $^{17}\text{O}(p, \gamma)^{18}\text{F}$  is set equal to 0.1, as suggested by the authors. In principle, the parameter  $f$  should be calibrated against chemical abundances in real stars.

Finally, the screening factors are from Graboske et al. (1973) and the  $\beta^+$ -decays are assumed to take place instantaneously.

### 5.3. The third dredge-up

The analytical treatment of the third dredge-up is described in Marigo et al. (1996), to whom the reader should refer for more details. Suffice it to remind that we describe this process with the aid of two basic parameters, namely:

- \*  $M_c^{\text{min}}$ , the minimum core mass for the third dredge-up to occur;
- \*  $\lambda = \Delta M_{\text{dredge}} / \Delta M_c$ , the efficiency of the third dredge-up, defined as the fraction of the core mass increment,  $\Delta M_c$ , during the previous inter-pulse period, that is brought up to the surface ( $\Delta M_{\text{dredge}}$  is the dredged-up mass).

Both parameters ( $M_c^{\text{min}} = 0.58 M_{\odot}$ ;  $\lambda = 0.65$ ), have been calibrated on the observed luminosity function of carbon stars of the LMC (Richer et al. 1979, Blanco et al. 1980, Cohen et al. 1981; see also Groenewegen & de Jong 1993 for similar theoretical results).

For the sake of simplicity, we do not consider the possible dependence of  $M_c^{\text{min}}$  and  $\lambda$  on the stellar mass and chemical composition. However, full calculations of the third dredge-up actually suggest that this process is favoured at lower metallicities and larger envelope masses (Wood 1981; Boothroyd & Sackmann 1988c).

In our model the third dredge-up is considered during the TP-AGB phase if two conditions are simultaneously met: i) the star has a core with a mass  $M_c > M_c^{\text{min}}$  and, ii) the corresponding thermal pulse has already reached the full amplitude regime. Moreover, we assume that the dredge-up events occur till the end of the TP-AGB evolution (*case A*). The adopted chemical composition (in mass fraction) of the inter-shell material just before the inward penetration of the convective envelope consists of  $^4\text{He}$  (76 %),  $^{12}\text{C}$  (22 %) and  $^{16}\text{O}$  (2 %) (Boothroyd &

Sackmann 1988c). Recently, Herwig et al. (1997) have shown that the introduction of additional partial mixing in the treatment of the third dredge-up may lead to significantly changed inter-shell abundances (e.g.  $^4\text{He}$  (25 %),  $^{12}\text{C}$  (50 %) and  $^{16}\text{O}$  (25%)).

Our simple treatment of the third dredge-up is mainly justified by the unsatisfactory understanding of the third dredge-up phenomenon even in stellar models that carefully follow thermal pulses. On one hand most authors still do not find significant dredge-up in their calculations (Vassiliadis & Wood 1993; Wagenhuber 1996), or assume the efficiency  $\lambda$  as an input quantity to be fixed by suitable calibrations (Forestini & Charbonnel 1997). On the other hand, the difficulty of too poor a dredge-up in low-mass stars seem to be overcome to some extent (Boothroyd & Sackmann 1988c; Frost & Lattanzio 1996; Straniero et al. 1997, Herwig et al. 1997), but extensive calculations over a wider range of stellar masses and metallicities are required in order to derive quantitative predictions which can be readily used in analytical models.

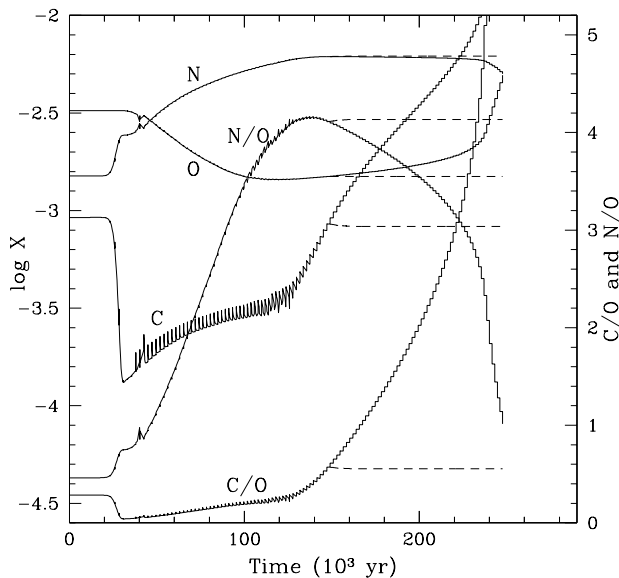


**Fig. 10.** Evolution of the surface abundances (by mass) of C, N, O and their ratios for the  $5.0M_{\odot}$ ,  $[Y = 0.25, Z = 0.008]$  TP-AGB star. The solid lines refer to *case A*, whereas the dashed lines describe the final freezing of the abundances in *case B*. See the text for further explanation.

In Fig. 10 we plot the time evolution of the surface abundances of C, N, and O for the  $5.0M_{\odot}$ ,  $[Y = 0.25, Z = 0.008]$  star, starting from the onset of the thermally pulsing regime till the complete ejection of the envelope. The saw-like trend of the C abundance is caused by the combined effect of the dredge-up episodes at each flash – clearly visible in the sudden spikes –, and envelope burn-

ing during the subsequent inter-flash period, which rapidly converts C into N.

Note that for most of the lifetime a TP-AGB star is expected to be oxygen-rich, in agreement with the observational indication of the most luminous AGB stars (see Sects. 4.4 and 5.1). In this case, the transition to a carbon star eventually happens when envelope burning is extinguished, and  $^{12}\text{C}$  enrichment due to convective dredge-up becomes dominant. Very recent observations (van Loon et al. 1997) in N-band and near-infrared photometry, aimed to detect dust-enshrouded AGB stars in the LMC, indicate that very luminous carbon stars ( $M_{\text{bol}} \sim -6.8$ ) are quite rare, but not absent.

Actually, spectroscopic estimates of the abundances in Planetary Nebulae (PN) indicate that high values of the ratios ( $\text{N}/\text{O} > 0.5$ ) and ( $\text{He}/\text{H} > 0.125$ ) typical of Type I PN are associated with rather low C/O ratios (in general  $\text{C}/\text{O} < 1$ ).

To investigate the effect of a different prescription we draw in Fig. 10 the dashed horizontal lines corresponding to the situation of a concomitant shut-down of the third dredge-up when envelope burning extinguishes (*case B*). In this case the formation of the carbon star is inhibited, and the final value of the C/O ratio is approximately 0.55, closer to the value in Type I PN.

These simple experiments are interesting in view of exploring different effects, without leading to draw definitive conclusions. Indeed, the competition between dredge-up and envelope burning is a crucial point that has not yet been solved by full AGB calculations, due to the uncertainties in the treatment of convection (as already mentioned), and additionally on the envelope mass, i.e. on mass-loss. Therefore, the critical envelope masses for the shut-down of dredge-up and envelope burning, respectively, are not known exactly up to now. In the case of the  $6M_{\odot}$ ,  $Z = 0.02$  model of Lattanzio & Boothroyd (1997) envelope burning seems to extinguish earlier than the dredge-up episodes do. Our *case A* resembles this situation.

For each model star in Table 1 we report the critical envelope mass,  $M_{\text{env}}^{\text{crit}}$ , at which hot-bottom burning is found to be no longer operative (e.g. when the contribution to the total luminosity falls below 1%) and the number of the dredge-up episodes occurred beyond this point according to *case A*.

#### 5.4. Type I Planetary Nebulae: how to get high He/H ?

Chemical abundances of PN in the Galaxy and Magellanic Clouds are an important observational constraint on prescriptions for nucleosynthesis, mixing, and mass-loss used to calculate the evolution of low- and intermediate-mass stars.

In the following, we will limit ourselves to address the question of the high overabundances of helium ( $\text{He}/\text{H} > 0.125$ ) and nitrogen ( $\text{N}/\text{O} > 0.5$ ) detected in Type I PN.

**Table 1.** Envelope mass,  $M_{\text{env}}^{\text{crit}}$ , at the extinction of envelope burning (when present) and corresponding inter-pulse number,  $N_{\text{P}}$ . This stage is defined as soon as  $L_{\text{EB}}/L < 0.01$ .  $\Delta N_{\text{P}}$  indicates how many dredge-up events happen beyond this point till the end of calculations (*case A*).

Z	$M(M_{\odot})$	$M_{\text{env}}^{\text{crit}}(M_{\odot})$	$N_{\text{P}}$	$\Delta N_{\text{P}}$
0.008	4.0	2.417	117	57
	4.5	2.365	86	60
	5.0	2.221	59	70
Z	$M(M_{\odot})$	$M_{\text{env}}^{\text{crit}}(M_{\odot})$	$N_{\text{P}}$	$\Delta N_{\text{P}}$
0.02	4.0	no envelope burning		
	4.5	3.053	15	41
	5.0	2.679	30	53

According to the present understanding (Renzini & Voli 1981; Groenewegen & de Jong 1994), high values of nitrogen would mainly be the result of envelope burning in massive AGB stars (the contribution from the first and second dredge-up being marginal).

This indication is confirmed by our results (*case B*) shown in the top panel of Fig. 11, where the N/O ratio attained after the second dredge-up eventually increases to considerable values during the TP-AGB evolution in partial agreement with the observations. In the case of the 4.5, and  $5.0M_{\odot}$ ,  $[Y = 0.25, Z = 0.008]$  stars the predicted N/O ratios exceed, roughly by a factor of two, the upper boundary ( $\log N/O \sim 0.5$ ) set by measurements of chemical abundances in PN of the LMC. The corresponding final C/O ratios (bottom-panel of Fig.11) are also consistent with observations. The low values ( $C/O < 1$ ) are the result of envelope burning rapidly converts carbon into nitrogen. In addition to this, the observational data seem also to suggest that during the final stages of the TP-AGB evolution the third dredge-up is likely to vanish, thus keeping low the C/O ratio (see Fig. (10)).

As far as the helium content is concerned, one can immediately notice in Fig. 11 that none of our results extends beyond  $\text{He}/\text{H} \sim 0.14$ , whereas the observational estimates can be as high as  $\sim 0.2$ .

Several experiments are performed to understand the reason of the marginal disagreement:

(1) With the present prescriptions a more efficient envelope burning (for instance obtained by increasing the mixing length parameter) can be ruled out as a larger production of helium also implies a significant increase of nitrogen, thus easily exceeding the upper limit on the N/O ratio indicated by the observations.

(2) High values of  $\text{He}/\text{H}$  could be obtained by letting the third dredge-up proceed till the very end of the TP-AGB phase (*case A*). In such a case, however, ratios C/O is expected to get  $\gg 1$ , in contrast with the observational

data. It is worth noticing that a successful situation might occur if only few dredge-up events (contrary to our *case A*, see Table 1) follow the cessation of envelope burning, so that C/O could remain smaller than unity.

(3) Under the assumptions of *case B* (i.e. the dredge-up episodes cease when envelope burning extinguishes), we investigate the effect of increasing the efficiency of the third dredge-up (e.g. setting  $\lambda = 0.9$ ). This actually leads to higher helium abundances, but always well below the observational value of  $\text{He}/\text{H} > 0.15$ .

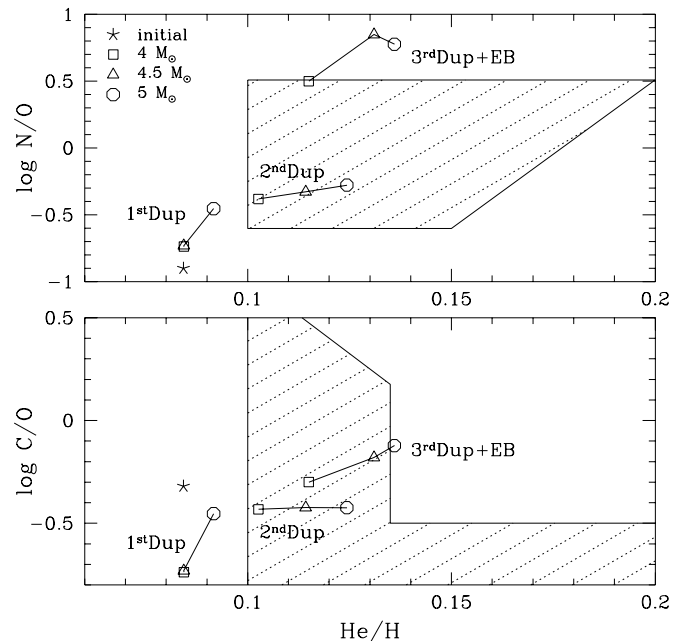


**Fig. 11.** N/O ratio (top-panel) and C/O ratio (bottom-panel) as a function of  $\text{He}/\text{H}$  for the 4.0, 4.5,  $5.0M_{\odot}$ ,  $[Y = 0.25, Z = 0.008]$  stars calculated according to the prescription of *case B*. The abundances are expressed as fractions by number. The three lines connecting the series of symbols (one for each value of the stellar mass as indicated) correspond to three theoretical abundances: 1) after the first dredge-up, 2) after the second dredge-up, 3) mass-averaged in the ejecta during the last  $5 \times 10^4$  yr before the end of the AGB phase. The asterisks refer to the initial abundance ratios. The dashed areas roughly correspond to the observed domain of type-I PNe in the LMC.

(4) Finally, we explore the possibility of a much deeper penetration of the convective envelope during the second dredge-up. Let us consider the case of the  $5.0M_{\odot}$ ,  $[Y = 0.25, Z = 0.008]$  star. The second dredge-up makes the surface ratio (by number)  $\text{He}/\text{H}$  to increase from  $\sim 0.092$  up to  $\sim 0.124$ . Correspondingly, the hydrogen  $Y_{\text{H}}$  and helium  $Y_{\text{He}}$  abundances (by number) change from ( $Y_{\text{H}}^1 \sim 0.726$ ,  $Y_{\text{He}}^1 \sim 0.066$ ) to ( $Y_{\text{H}}^2 \sim 0.662$ ,  $Y_{\text{He}}^2 \sim 0.082$ ), where the superscripts 1 and 2 refer to the values just

before and after the second dredge-up, respectively. The dredged-up mass (in  $M_\odot$ ) is given by:

$$\Delta M_{2D} = M(Q_{XY} - Q_{\text{conv}}^{\text{max}}) \quad (19)$$

where  $M$  (in  $M_\odot$ ) is the total stellar mass,  $Q_{XY} \sim 0.252853$  defines the  $X - Y$  discontinuity when the H-burning shell extinguishes, and  $Q_{\text{conv}}^{\text{max}} \sim 0.186333$  corresponds to the maximum penetration of the envelope convection during the dredge-up, with  $Q = M_r/M$  (mass coordinate). In this case,  $\Delta M_{2D}$  amounts to  $0.3326M_\odot$ .

With aid of the above quantities, we can evaluate the maximum amount of material,  $\Delta M_{2D}^{\text{max}}$  that can be dredged-up if the envelope extends down to the upper boundary ( $Q_{\text{He}} \sim 0.184678$ ) of the He-burning shell, which is an insuperable barrier to the inward displacement of the convection. The dredged-up material is

$$\Delta M_{2D}^{\text{max}} = M(Q_{XY} - Q_{\text{He}}) \quad (20)$$

which gives  $\Delta M_{2D}^{\text{max}} = 0.3410M_\odot$ . Note that this value slightly exceeds the actual value already calculated with Eq. (19).

For the sake of comparison, we estimate also the amount of mass,  $\Delta M'_{2D}$ , that should be dredged-up in order to get the typically high values of the helium content measured in Type-I PN. As an example, let us consider the case of  $\text{He}/\text{H} \sim 0.176$ , or equivalently  $Y_{\text{H}}^{2'} \sim 0.582$ ,  $Y_{\text{He}}^{2'} \sim 0.1025$ . Denoting by  $Y_{\text{He}}^{\text{d}} \sim (1 - Z)/4 = 0.248$  the helium abundance (by number) in the dredge-up material, and  $M_{\text{env}} = M(1 - Q_{XY}) \sim 3.73M_\odot$  the mass of the convective envelope just before the penetration, we have:

$$\Delta M'_{2D} = M_{\text{env}} \frac{Y_{\text{He}}^1 - Y_{\text{He}}^{2'}}{Y_{\text{He}}^{2'} - Y_{\text{He}}^{\text{d}}} \quad (21)$$

Equation (21) yields  $\Delta M'_{2D} \sim 0.93M_\odot$ , which is higher than the actual value by a factor of almost three and, above all, it largely exceeds the maximum value allowed,  $\Delta M_{2D}^{\text{max}}$ .

Similar estimates, carried out for the other star masses considered in this paper, lead us to the conclusion that in order to get high values of the  $\text{He}/\text{H}$  ratio ( $> 0.16$ ) the second dredge-up cannot play the prevalent role.

All things considered, we expect that the dominant causes of helium enrichment are nucleosynthesis and mixing occurring during the TP-AGB phase and, mainly, cumulative effects of recurrent dredge-up episodes.

### 5.5. Secondary and primary synthesis of CNO nuclei

During the TP-AGB evolution of stars undergoing envelope burning, at each dredge-up event some primary  $^{12}\text{C}$  and  $^{16}\text{O}$  nuclei (produced by  $\alpha$ -capture reactions) are injected into the envelope where they can partake in the CNO cycle for the conversion of hydrogen into helium. Therefore, as a consequence of chemical pollution by the

third dredge-up and subsequent nuclear burning at the base of the envelope, the surface distribution of the CNO nuclei consists of two components:

- A *secondary component* produced by nuclear reactions involving only seed metals originally present in the star at the epoch of its formation;
- A *primary component* synthesized by a chain of nuclear burnings beginning from H and He and hence independent of the original metal content.

The surface abundance (by number)  $Y_i$  of any element  $i$  of the CNO group at time  $t$ , can be expressed as  $Y_i = Y_i^{\text{S}} + Y_i^{\text{P}}$ , where  $Y_i^{\text{S}}$  and  $Y_i^{\text{P}}$  are the secondary and primary fractions, respectively. At the time  $t' = t + dt$ , because of nuclear burning at the base of the convective envelope, the element  $i$  will achieve a new surface abundance  $Y_i' = Y_i^{\text{S}'} + Y_i^{\text{P}'}$ , with a different relative partition of the two components.

The method to follow the time evolution of both the secondary and primary nuclear synthesis is quite simple, in virtue of the following considerations. The generic form of the differential equation describing the time variation of the abundance  $Y_i$  can be written as:

$$\frac{dY_i}{dt} = \sum_j (\pm) R_{ij} Y_{\text{H}} Y_i \quad (22)$$

or equivalently,

$$\frac{d(Y_i^{\text{S}} + Y_i^{\text{P}})}{dt} = \sum_j (\pm) R_{ij} Y_{\text{H}} (Y_i^{\text{S}} + Y_i^{\text{P}}) \quad (23)$$

where the summation is performed over all the nuclear reactions that create the element (sign +) and destroy it (sign -), and the various  $\beta$ -decays are neglected. Two important points are to be noticed: i) the nuclear rates  $R_{ij}$  are functions of temperature and density only, and ii) the CNO nuclei react only with protons and not among each other. This latter condition is clearly expressed by the product  $Y_{\text{H}} Y_i$  in Eq. (22), where  $Y_{\text{H}}$  is the hydrogen abundance. Since the only possible reactions are proton-captures on CNO nuclei it follows that in Eq. (23) mixed products of secondary and primary abundances (e.g.  $Y_i^{\text{S}} Y_j^{\text{P}}$ ) are not possible. Therefore, Eq. (23) can be properly split into two independent equations:

$$\frac{dY_i^{\text{S}}}{dt} = \sum_j (\pm) R_{ij} Y_{\text{H}} Y_i^{\text{S}} \quad (24)$$

$$\frac{dY_i^{\text{P}}}{dt} = \sum_j (\pm) R_{ij} Y_{\text{H}} Y_i^{\text{P}} \quad (25)$$

which can be integrated separately over the time  $dt$  to give the new secondary  $Y_i^{\text{S}'}$  and primary  $Y_i^{\text{P}'}$  fractions, such that  $Y_i^{\text{S}'} + Y_i^{\text{P}'} = Y_i'$ . In other words, the differential

**Table 2.** Chemical abundances (in mass fraction) in stars with initial mass  $M_i$  and original metallicity  $Z = 0.008$  at three stages, namely: i) at the zero-age main sequence (Initial); ii) soon after the first dredge-up (1 D); and iii) soon after the second dredge-up (2 D).

	H	$^3\text{He}$	$^4\text{He}$	$^{12}\text{C}$	$^{13}\text{C}$	$^{14}\text{N}$	$^{15}\text{N}$	$^{16}\text{O}$	$^{17}\text{O}$	$^{18}\text{O}$	
Initial	0.7420	2.675E-05	0.2500	1.371E-03	1.652E-05	4.238E-04	1.672E-06	3.851E-03	1.560E-06	8.680E-06	
1 D	$M_i$										
	4.0	0.7417	1.125E-04	0.2503	1.167E-03	5.927E-05	6.167E-04	1.055E-06	3.850E-03	1.607E-06	8.331E-06
	4.5	0.7417	9.285E-05	0.2502	1.160E-03	5.729E-05	6.263E-04	1.044E-06	3.850E-03	1.631E-06	8.249E-06
	5.0	0.7259	6.845E-05	0.2661	9.833E-04	4.765E-05	1.098E-03	9.139E-07	3.559E-03	3.196E-06	7.003E-06
2 D	$M_i$										
	4.0	0.7032	9.179E-05	0.2887	9.164E-04	4.959E-05	1.261E-03	8.402E-07	3.459E-03	4.623E-06	6.595E-06
	4.5	0.6809	7.394E-05	0.3111	9.039E-04	4.871E-05	1.379E-03	8.238E-07	3.342E-03	4.197E-06	6.445E-06
	5.0	0.6625	5.991E-05	0.3295	8.756E-04	4.654E-05	1.502E-03	8.052E-07	3.243E-03	3.691E-06	6.219E-06

**Table 3.** The same as in Table 2, but with initial metallicity  $Z = 0.02$ .

	H	$^3\text{He}$	$^4\text{He}$	$^{12}\text{C}$	$^{13}\text{C}$	$^{14}\text{N}$	$^{15}\text{N}$	$^{16}\text{O}$	$^{17}\text{O}$	$^{18}\text{O}$	
Initial	0.7000	2.996E-05	0.2800	3.427E-03	4.130E-05	1.060E-03	4.180E-06	9.626E-03	3.900E-06	2.170E-05	
1 D	$M_i$										
	4.0	0.6778	8.915E-05	0.3021	2.420E-03	1.222E-04	2.687E-03	2.262E-06	9.003E-03	1.599E-05	1.749E-05
	4.5	0.6776	7.410E-05	0.3022	2.444E-03	1.254E-04	2.690E-03	2.253E-06	8.966E-03	1.358E-05	1.764E-05
	5.0	0.6986	6.937E-05	0.2814	2.692E-03	1.372E-04	1.885E-03	2.408E-06	9.546E-03	8.416E-06	1.937E-05
2 D	$M_i$										
	4.0	0.6713	8.684E-05	0.3087	2.363E-03	1.221E-04	2.839E-03	2.197E-06	8.906E-03	1.738E-05	1.713E-05
	4.5	0.6485	6.961E-05	0.3314	2.305E-03	1.230E-04	3.189E-03	2.123E-06	8.586E-03	1.446E-05	1.665E-05
	5.0	0.6307	5.830E-05	0.3494	2.282E-03	1.241E-04	3.432E-03	2.072E-06	8.341E-03	1.218E-05	1.633E-05

equation (23) can be seen as a linear transformation<sup>1</sup> of the variables  $Y_i^S$  and  $Y_i^P$ .

In Figs. 12 and 13 the evolution of secondary and primary  $^{12}\text{C}$ ,  $^{13}\text{C}$ ,  $^{14}\text{N}$ ,  $^{15}\text{N}$ ,  $^{16}\text{O}$ ,  $^{17}\text{O}$ ,  $^{18}\text{O}$  surface abundances (by mass) is plotted as a function of time for the  $4.5M_\odot$  TP-AGB star with  $[Y = 0.25, Z = 0.008]$ . It can be noticed that for a few CNO nuclei (e.g.  $^{12}\text{C}$ ,  $^{13}\text{C}$ ,  $^{14}\text{N}$ , and  $^{15}\text{N}$ ), the primary component (which is initially equal to zero by definition) of the surface abundance grows until it overcomes the secondary one.

## 6. Yields of chemical elements

Tables 4 and 5 give the chemical yields from stars which experience envelope burning. The initial masses and chem-

<sup>1</sup> We recall that a function  $f(x, y)$  is a linear transformation if  $f(ax + by) = af(x) + bf(y)$ .

ical compositions are  $4.0, 4.5, 5.0M_\odot$  and  $[Y = 0.28, Z = 0.02]$  and  $[Y = 0.25, Z = 0.008]$ . These data complete the sets of chemical yields from lower mass stars ( $0.7 < M/M_\odot \leq 4.0$ ) already presented by Marigo et al. (1996). The “old” results for the  $4.0M_\odot$  models in Marigo et al. (1996) should be replaced with the “new” results of this study. For each elemental species  $i$  we calculate the amount of mass  $M_y(i)$  which is newly synthesized by nuclear burning in the star and returned to the interstellar medium during the entire lifetime ( $T$ ):

$$M_y(i) = \int_0^T [X(i) - X^0(i)] \frac{dM}{dt} dt \quad (26)$$

where  $X(i)$  and  $X^0(i)$  are the current and the initial surface abundance, respectively;  $dM/dt$  is the current mass-loss rate.

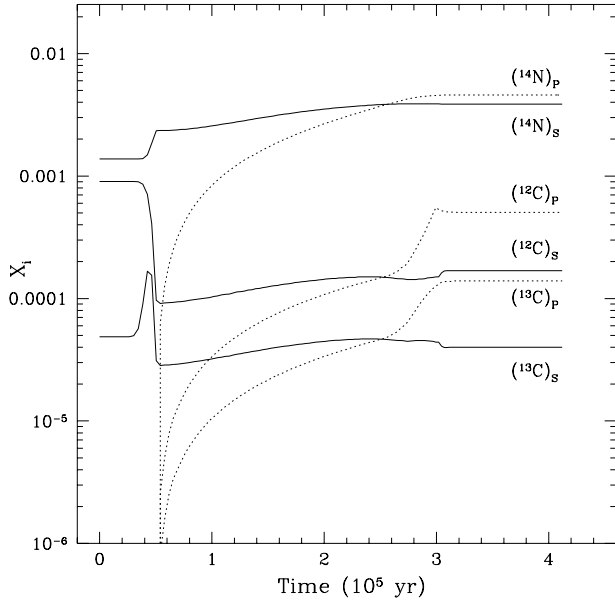


**Fig. 12.** Secondary and primary surface abundances (by mass) of  $^{12}\text{C}$ ,  $^{13}\text{C}$ , and  $^{14}\text{N}$  as a function of time for the  $4.5M_{\odot}$ ,  $[Y = 0.25, Z = 0.008]$  star in the TP-AGB phase (*case B*).

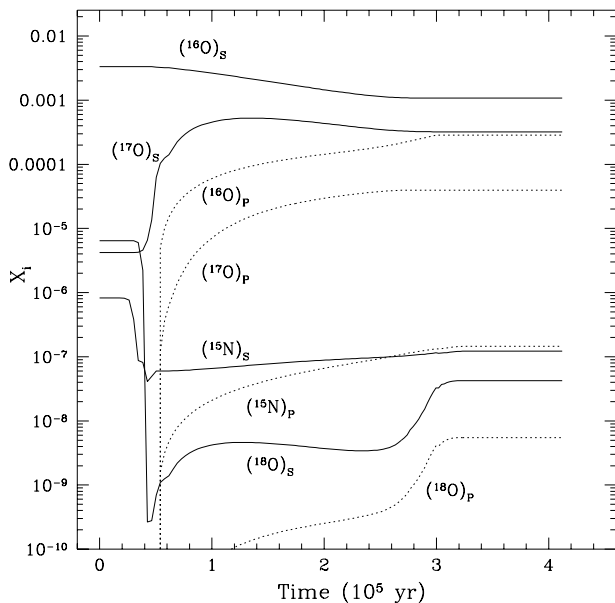


**Fig. 13.** The same as in Fig. 12, but for the surface abundances of  $^{15}\text{N}$ ,  $^{16}\text{O}$ ,  $^{17}\text{O}$ , and  $^{18}\text{O}$  (*case B*).

It is worth recalling that with the adopted mass-loss rates along the TP-AGB phase (Vassiliadis & Wood 1993), the reduction of stellar mass during the E-AGB is indeed negligible.

As far as the CNO nuclei are concerned, the entry  $M_y(\text{CNO})$  in Table 4 corresponds to the total yield of all the isotopes, whereas the entries of Table 5 explicitly gives both the secondary and primary yield for each element. These are calculated with:

$$M_y^S(i) = \int_0^T [X^S(i) - X^0(i)] \frac{dM}{dt} dt \quad (27)$$

$$M_y^P(i) = \int_0^T X^P(i) \frac{dM}{dt} dt \quad (28)$$

The total yield of any element is simply  $M_y = M_y^S(i) + M_y^P(i)$ .

According to the above definitions, the primary yields can be only  $\geq 0$ , whereas secondary yields can be either  $\geq 0$  or  $< 0$ , in the respective cases that the mass-averaged abundance of the element in the ejecta is greater, equal or smaller than its original value at the formation of the star.

The reader should refer also to Tables 2 and 3 for an easier understanding of the effects on the surface abundances caused by different mixing episodes during the evolution of the star. Suffice it to recall that the both the first and second dredge-up affect (by increasing or decreasing) only the secondary components of the CNO surface abundances. In fact, in these cases the envelope is polluted by material which has undergone CNO-cycling of nuclei synthesized from metal seeds originally present in the star.

From a general analysis of the total yields and their components (primary versus secondary) it turns out that three alternatives are possible:

1.  $M_y^S(i) > 0$  and  $M_y^P(i) > 0$  so that  $M_y > 0$
2.  $M_y^S(i) < 0$  and  $M_y^P(i) > 0$  so that  $M_y > 0$
3.  $M_y^S(i) < 0$  and  $M_y^P(i) > 0$  so that  $M_y < 0$

The first case applies, for instance, to the  $^{13}\text{C}$  abundance which is significantly enhanced by the first dredge-up (secondary origin), and subsequently by envelope burning, thanks to proton-capture reactions on  $^{12}\text{C}$  nuclei (secondary and primary nucleosynthesis). It results that the primary yield of  $^{13}\text{C}$  exceeds (by few factors, depending on the efficiency of envelope burning) the secondary contribution in all the stars under consideration, but for the  $4.0M_{\odot}$ ,  $[Y = 0.28, Z = 0.02]$  star, in which the effect of the first dredge-up prevails. Likewise, the relative weight of the secondary and primary components on the total yield of  $^{14}\text{N}$  depends on the interplay between the secondary enrichment due to the first and second dredge-up episodes, and the primary contribute given by the CNO-cycle during envelope burning. The highest value of  $M_y^P(^{14}\text{N})$  is produced by the  $4.0M_{\odot}$ ,  $[Y = 0.25, Z = 0.008]$  star, in which envelope burning has been active for the longest time.



**Table 4.** Total yields (in  $M_{\odot}$ ) from intermediate-mass stars with initial metallicity  $Z$ , and mass  $M_i$  (*case A*). The amount of mass,  $M_{\text{ej}}$ , ejected over the entire evolution, and the final mass of the core,  $M_f$ , are indicated in solar units.

$Z$	$M_i$	$M_{\text{ej}}$	$M_f$	$M_y(\text{H})$	$M_y(^3\text{He})$	$M_y(^4\text{He})$	$M_y(\text{CNO})$
0.008	4.0	3.059	0.941	-2.218E-01	-8.130E-05	1.877E-01	3.386E-02
	4.5	3.545	0.955	-3.374E-01	-9.478E-05	3.138E-01	2.363E-02
	5.0	4.018	0.982	-4.024E-01	-1.075E-04	3.885E-01	1.453E-02
0.02	4.0	3.143	0.857	-1.121E-01	1.594E-04	1.087E-01	8.798E-03
	4.5	3.604	0.896	-2.178E-01	-7.890E-05	2.059E-01	1.202E-02
	5.0	4.061	0.939	-3.257E-01	-1.188E-04	3.129E-01	1.379E-02

**Table 5.** Total yields from intermediate-mass stars (*case A*). The notation is the same as in Table 4. For each isotope of the CNO group, the secondary (S) and primary (P) yields are distinguished.

$Z$	$M_i$	$M_{\text{ej}}$	$M_f$	S/P	$M_y(^{12}\text{C})$	$M_y(^{13}\text{C})$	$M_y(^{14}\text{N})$	$M_y(^{15}\text{N})$	$M_y(^{16}\text{O})$	$M_y(^{17}\text{O})$	$M_y(^{18}\text{O})$
0.008	4.0	3.059	0.941	S	-3.884E-03	3.546E-05	5.540E-03	-4.905E-06	-2.735E-03	8.199E-04	-2.645E-05
				P	8.014E-03	4.845E-04	2.307E-02	7.100E-07	2.422E-03	1.246E-04	1.532E-08
	4.5	3.545	0.955	S	-4.336E-03	9.594E-05	1.195E-02	-5.532E-06	-9.652E-03	1.179E-03	-3.068E-05
				P	7.741E-03	3.601E-04	1.475E-02	4.369E-07	1.452E-03	1.333E-04	1.157E-08
	5.0	4.018	0.982	S	-4.855E-03	1.266E-04	1.377E-02	-6.281E-06	-1.099E-02	1.299E-03	-3.481E-05
				P	7.177E-03	2.439E-04	6.697E-03	1.947E-07	1.046E-03	5.667E-05	3.951E-09
0.02	4.0	3.143	0.857	S	-3.503E-03	3.298E-04	5.516E-03	-1.253E-05	-2.556E-03	4.230E-05	-1.834E-05
				P	8.235E-03	1.411E-05	3.327E-07	8.870E-12	7.498E-04	1.689E-09	1.797E-14
	4.5	3.604	0.896	S	-1.090E-02	2.801E-04	1.545E-02	-1.447E-05	-4.414E-03	3.098E-04	-7.802E-05
				P	8.743E-03	3.028E-04	1.415E-03	4.364E-08	9.299E-04	9.966E-07	1.068E-10
	5.0	4.061	0.939	S	-1.263E-02	1.879E-04	1.980E-02	-1.628E-05	-9.853E-03	3.293E-03	-8.791E-05
				P	8.345E-03	2.184E-04	3.489E-03	1.035E-07	1.033E-03	1.469E-05	9.511E-10

It is worth remarking that intermediate-mass stars with  $M \geq 4.0M_{\odot}$  are a source of primary  $^{14}\text{N}$  for the chemical enrichment of the interstellar medium. These stars could play an important role in view of interpreting, with the aid of chemical evolutionary models of galaxies, the observed trend of the data in the  $\log(\text{N}/\text{O})$  vs.  $\log(\text{O}/\text{H})$  plane, which suggests the existence of a significant primary component of  $^{14}\text{N}$  (see Matteucci 1997). A positive yield is predicted also for  $^{17}\text{O}$ , thanks to the first dredge-up which increases the secondary surface abundance, and to CNO-cycling of primary nuclei during envelope burning.

The second case applies to  $^{12}\text{C}$ , for which the surface abundance is first decreased as a consequence of both the first and second dredge-up episodes, and then increased thanks to the convective dredge-up at thermal pulses. In all the stars considered, the positive net yield  $M_y(^{12}\text{C})$  is of primary origin only.

Finally, the third case refers to the other CNO isotopes ( $^{15}\text{N}$ ,  $^{16}\text{O}$ , and  $^{17}\text{O}$ ), for which the negative contribution of the secondary component exceeds the positive one of primary nature. It follows that for these elements no chemical enrichment of the interstellar medium is expected from the stars under consideration. We notice that as far as  $^{16}\text{O}$  is concerned,  $M_y^{\text{P}}(^{16}\text{O})$  crucially depends on the number of dredge-up episodes that occurred during the TP-AGB phase. The  $4.0M_{\odot}$ , [ $Y = 0.25, Z = 0.008$ ] model star – which experiences the greatest number of thermal pulses – produces a primary yield nearly as high as the secondary one.

## 7. Concluding remarks

In this study we have developed an original method to follow the TP-AGB evolution of stars with envelope burning. To this aim we formulated a suitable model for static envelopes, in which the equation of energy balance is in-

cluded. The structure of the envelope is then solved in details with the aid of two boundary conditions having a general validity, so that the new algorithm can be applied also to the case with no envelope burning. The method we are proposing is very flexible and it can be employed to investigate different questions concerning the occurrence of envelope burning.

Among other results, we draw attention on the problem raised by the high values of helium content in Type-I PN, which cannot find an easy explanation without violating the observational abundances of nitrogen. This is an important conclusion setting strong constraints not only on nucleosynthesis, but also on other evolutionary aspects of AGB stars, e.g. mass-loss,  $M_c - L$  relation, lifetimes, distribution on the H-R diagram, and pulsational properties.

*Acknowledgements.* Many thanks to Léo Girardi for providing the results of evolutionary calculations, and for constructive discussions. We are grateful to our referee for many interesting and useful remarks. This study has been financed by the Italian Ministry of University, Scientific Research and Technology (MURST), the Italian Space Agency (ASI), and the European Community under TMR grant ERBFMRX-CT96-0086.

## References

- Alongi M., Bertelli G., Bressan A. et al., 1993, A&AS 97, 851  
 Alexander D.R., Ferguson J.W., 1994 ApJ 437, 879  
 Bessel M.S., Wood P.R., Lloyd Evans T., 1983, M.N.R.A.S. 202, 59  
 Blanco V.M., McCarthy M.F., Blanco B.M., 1980, ApJ 242, 938  
 Blöcker T., 1995a, A&A 297, 727  
 Blöcker T., 1995b, A&A 299, 755  
 Blöcker T., Schönberner D., 1991, A&A 244, L43  
 Boothroyd A.I., Sackmann I.-J., 1988a, ApJ 328, 641  
 Boothroyd A.I., Sackmann I.-J., 1988b, ApJ 328, 653  
 Boothroyd A.I., Sackmann I.-J., 1988c, ApJ 328, 671  
 Boothroyd A.I., Sackmann I.-J., 1992, ApJ 393, L21  
 Boothroyd A.I., Sackmann I.-J., Ahern S.C., 1993, ApJ 416, 762  
 Cameron A.G.W., Fowler W.A., 1971, ApJ 164, 111  
 Caughlan, G.R., Fowler, W.A., 1988, Atomic Data Nuc. Data Tables 40, 283  
 Clayton D.D., 1983, Principles of Stellar Evolution and Nucleosynthesis, University of Chicago Press, Chicago and London  
 Cohen J.G., Frogel J.A., Persson S.E., Elias J.H., 1981, ApJ 249, 481  
 Costa E., Frogel J.A., 1996, AJ 112, 2607  
 Eggleton P.P., 1967, MNRAS 135, 243  
 Forestini M., Charbonnel C., 1997, A&AS 123, 241  
 Frost C.A., Lattanzio J.C., 1996, ApJ 473, 383  
 Graboske H.C., Witt H.E., Grossman A.S., Cooper, M.S., 1973, ApJ 181, 457  
 Groenewegen M.A.T., de Jong T., 1993, A&A 267, 410  
 Groenewegen M.A.T., de Jong T., 1994, A&A 282, 127  
 Harris M.J., Lambert D.L., Smith V.V. 1985, ApJ 299, 375  
 Harris M.J., Lambert D.L., Hinkle K.H., Gustafsson B., Eriksson K., 1987, ApJ 316, 294  
 Harris M.J., Lambert D.L., Smith V.V. 1988, ApJ 325, 768  
 Havazelet D., Bakart Z., 1979, ApJ 233, 589  
 Herwig F., Blöcker T., Schönberner D., El Eid M., 1997, A&A 324, L81  
 Hughes S.M.G., Wood P.R., 1990, AJ 99, 784  
 Iben I., 1973, ApJ 185, 209  
 Iben I. 1977, ApJ 217, 788  
 Iben I., Truran J.W., 1978, ApJ 220, 980  
 Iben I., Tutokov A.V. , 1984, ApJ 282, 615  
 Iglesias C.A., Rogers F.J., 1996, ApJ 464, 943  
 Köster D. , Schönberner D., 1986, A&A 154, 125  
 Lattanzio J.C., 1986, ApJ 311, 708  
 Lattanzio J.C., 1992, Proc. Astron. Soc. Austr. 10, 120  
 Lattanzio J.C., Boothroyd A.I., 1997, in Astrophysical Implications of the Laboratory Study of Presolar Materials, Bernatowitz T., Zinner E. (eds), AIP: Sunnyside, NY, in press  
 van Loon J.Th., Zijlstra A.A., Whitelock P.A., et al., 1997, A&A, in press  
 Marigo P., Bressan A., Chiosi C., 1996, A&A 313, 545  
 Marigo P., Girardi L., Chiosi C., 1997, A&A 316, L1  
 Matteucci F., 1997, Fund. Cosmic Physics, in press  
 Numerical Recipes, 1990, Press W.H., Flannery B.P., Teukolsky S.A., Vetterling, W.T., Cambridge University Press, Cambridge, New York, Port Chester, Melbourne, Sidney, pag. 251  
 Paczynski B., 1970, Acta Astr. 20, 47  
 Peimbert M., Torres-Peimbert S., 1983, IAU Symp. 103, 233  
 Reid N.L., Tinney C., Mould J., 1990, ApJ 348, 98  
 Reid N.L., Hughes S.M.G., Glass I.S., 1995, M.N.R.A.S. 275, 331  
 Renzini A., Voli M., 1981, A&A 94, 175  
 Richer H.B., Olander N., Westerlund B.E., 1979, ApJ 230, 724  
 Sackmann I.-J., Boothroyd A.I., 1991, ApJ 366, 529  
 Sackmann I.-J., Boothroyd A.I., 1992, ApJ 392, L71  
 Scalo J.M., Despain K.H., Ulrich R.K., 1975, ApJ 196, 805  
 Schönberner D., 1983, ApJ 272, 708  
 Smith V.V., Lambert D.L., 1985, ApJ 294, 326  
 Smith V.V., Lambert D.L., 1990, ApJ 361, L69  
 Smith V.V., Plez B., Lambert D.L., 1995, ApJ 441, 735  
 Straniero O., Chieffi A., Limongi M. et al., 1997, ApJ 478, 332  
 Sugimoto D., 1971, Prog. Theor. Phys. 45, 761  
 Tuchman Y., Sack N., Barkat Z., 1979, ApJ 234, 217  
 Tuchman Y., Glasner A., Barkat Z., 1983, ApJ 268, 356  
 Uus, U., 1972, Proc. IAU Colloquium No 17, Stellar Ages, ed. G.C. de Strobel and A.M. Delplace.  
 Vassiliadis E., Wood P.R., 1993, ApJ 413, 641  
 Wagenhuber J., 1996, PhD thesis, TU München  
 Westerlund B.E., Azzopardi M., Rebeirot E., Breysacher J., 1991, A&AS 91, 425  
 Wood P.R., 1981, in: Physical processes in red giants, Proc. of the Second Workshop, Erice, Italy (September 3-13, 1980), Dordrecht, D. Reidel Publishing Co., p. 135-139  
 Wood P.R., Zarro D.M., 1981, ApJ 247, 247  
 Wood P.R., Bessel M.S., Fox M.W., 1983, ApJ 272, 99  
 Wood P.R., Whiteoak J.B., Hughes S.M.G. et al., 1992, ApJ 397, 552